DALTON
FULL PAPER

A new antimetabolite, 5-morpholinomethyl-2-thiouracil—spectral properties, thermal profiles, antibacterial, antifungal and antitumour studies of some of its metal chelates †

P. Kamalakannan,[a] D. Venkappayya *[a] and T. Balasubramanian [b]

[a] *Department of Chemistry, Regional Engineering College, Tiruchirappalli-620015, India. E-mail: dvenka@rect.ernet.in*
[b] *Department of Physics, Regional Engineering College, Tiruchirappalli-620015, India*

Received 28th February 2002, Accepted 18th June 2002
First published as an Advance Article on the web 26th July 2002

A new antimetabolite of thymine, 5-morpholinomethyl-2-thiouracil (MMTU) has been synthesized *via* the Mannich reaction of 2-thiouracil, formaldehyde and morpholine. The product was chemically and structurally characterized using various techniques ranging from microelemental analysis to XRD studies. About thirteen metal ion complexes of MMTU have been isolated and were found to exhibit five different types of bonding pattern such as unidentate dimeric, bidentate, bidentate binuclear, tridentate binuclear and tetradentate binuclear. To gain theoretical support for the experimental findings regarding the donor atoms proposed based on spectral studies of the complexes semi-empirical quantum mechanical calculations were carried out using MOPAC. The anomalous behaviour exhibited by a few complexes was explained based on steric constraint and stabilization energy gain upon six membered chelate formation. Thermodynamic and kinetic parameters were evaluated. Antimicrobial, antifungal and antitumour studies have also been carried out. Structure, thermal stability and biological activity of the complexes have been correlated.

Introduction

The present objective is to synthesize a more potent antimetabolite and to explore preliminarily the possibility of its use in chemotherapy. This work is in continuation of our systematic study of the synthesis and characterization of new antimetabolites derived from pyrimidine and their metal ion complexes.[1–6] The substituted (especially at the 5 position) uracils and thiouracils are known to play a vital role in many metabolic processes[7–20] most of which are also mediated by metal ions.[21–23] Many of the drugs have been known to exhibit increased anticancer activity when administered as metal complexes.[24–27] Considering the structural requirements for significant cytotoxic activity, carrier moieties such as heterocyclic amines[28–33] have been introduced so as to readily react with plasma proteins. In particular, morpholine substituted anthracyclines and adriamycin have been found to show greater antitumour activity than the parent compound.[34,35] In view of the above it was considered appropriate to introduce morpholine through a methylene bridge at the 5 position of 2-thiouracil *via* the Mannich route and isolate the new product, MMTU. The thiouracils have the potential to bind to the metal ion through sulfur, nitrogen, oxygen or a combination of these.[36–39] Such bindings are likely to leave some potential donor atoms free and these free donor atoms enhance the biological activity. Apart from the thiouracil donor atoms, morpholine nitrogen and oxygen atoms can also act as binding sites. It was thus felt that the study of the interaction of metal ions with the above derivative would be useful in understanding the effect of free heteroatoms on biological activity.

† Electronic supplementary information (ESI) available: thermograms, infrared, NMR and mass spectra of MMTU; table comparing bond lengths in MMTU with other thiouracil derivatives; tables of data for MMTU including: least-squares plane calculations, hydrogen bond distances, results of the PM3 calculation, eigen values for the M.O. levels, A.O.[S] electron populations using the PM3 Hamiltonian, the bonding contribution of each M.O., dipole, point charge and hybrid values and net atomic charges and dipole contributions. See http://www.rsc.org/suppdata/dt/b2/b202127g/

Results and discussion

MMTU crystallised from methanol registers a single R_f value on an HPLC run confirming its purity. The compound melts at 208.3 °C with a heat of absorption of 103.3 J g^{-1}. The C, H, N and S analytical results were found to be 47.47, 5.71, 18.50, 14.23 and 14.09% respectively, which are in close agreement with the calculated values of 47.58, 5.73, 18.50, 14.10 and 14.10%. Elemental analysis indicates the molecular formula as $C_9H_{13}N_3O_2S$.

The UV-Vis spectrum of a 10^{-3} M MMTU in DMF registered bands at 260 and 290 nm which are assignable to the $n \longrightarrow \pi^*$ and $\pi \longrightarrow \pi^*$ transitions, respectively of the thiocarbonyl group. The above two bands occur at slightly longer wavelengths compared with those for 2-thiouracil[40] which indicates the derivatisation of the compound.

The IR spectrum of MMTU registers absorption bands at 3200 and 3140 cm^{-1} which are the split bands of a symmetric stretch of NH and the other bands at 3040 and 2960 cm^{-1} arise due to ν_{CH} of 'CH' and 'CH_2' groups, respectively. The sharp absorption bands at 1690, 1571 and 1473 cm^{-1} are due to $\nu_{C(4)O}$, $\delta_{N(1)H}$ and $\delta_{N(3)H}$, respectively. Compared with the IR spectrum of 2-thiouracil, a new sharp and intense band at 1102 cm^{-1} is seen which can be assigned to ν_{C-N-C} of the morpholine moiety. This band confirms the insertion of the amino moiety into thiouracil. The absorption band at 1225 cm^{-1} is assigned to $\nu_{C=S}$.

The ^1H NMR spectrum of MMTU (Fig. S1, ESI) in DMSO-d_6 contained four signals, two singlets and two doublets. Comparing this NMR spectrum with that for thiouracil,[41] it is observed that the resonance signal due to C(5)H is absent and three new signals are observed at highfield. The chemical shift values of the signals are δ 7.32 (s), 5.84 (s), 3.56 (t), 3.16 (s)

and 2.38 (t) which can be assigned to C(6)H, C(2)SH, $–(CH_2)_2–O$, $–CH_2–$ and $–N–(CH_2)_2–$, respectively. These signals evidence the incorporation of an aminomethyl moiety at the 5 position of 2-thiouracil. Offset scanning beyond δ 10 to capture the N(1)H and N(3)H resonances was unsuccessful due to the exceedingly fast exchange rates and therefore this proton could not be identified using the CW-60 MHz NMR spectrometer. However, in the FT-400 MHz NMR spectrometer the N(3)H signal appeared as a broad band at δ 12.10. The ^{13}C NMR signals at δ 176.111, 161.479, 140.167, 113.361, 105.362, 66.261 and 52.949 (Fig. S2, ESI) were assigned to C(2)SH, C(4)O, C(6)H, C(5)H, $N–(CH_2)_2$, $(CH_2)_2–O$ and $–CH_2–$ respectively. The observed carbon chemical shift values are in close agreement with the structure proposed on the basis of ^1H NMR data. The above observation is further substantiated by the fact that 2-thiouracil exists as the thiol rather than as the thione isomer.[42]

The solution state high resolution NMR spectrum exhibits a signal corresponding to the presence of N(3)H and the absence of N(1)H, whereas the solid state IR study indicates the presence of C(2)=S and N(1)H. It is therefore inferred that in the solid state MMTU exists in the thione form (I). In DMSO solution, it displays thione–thiol equilibrium, the latter being the predominant isomer.

The mass spectrum of MMTU (Fig. S3, ESI) exhibits a molecular ion peak at *m/z* 227 which corresponds to the proposed molecular mass of the compound. The likely fragmentation pattern of MMTU is depicted in the following scheme.

Molecular topology of MMTU

The crystal data and structure refinement parameters for MMTU are given in Table 9. An ORTEP view of MMTU with the atom numbering scheme is shown in Fig. 1. There are two pseudo-symmetric molecules with two water oxygens and two chlorides in the asymmetric unit. Table S1 (ESI) compares the bond lengths of MMTU with those of 5,6-dihydro-2-thiouracil,[43] 5,6-dihydrouracil,[44] 2,4-dithiouracil,[45] uracil[46] and 6-amino-2-thiouracil monohydrate.[47] The C(5)–C(6) distances of 1.339(8) Å for molecule A and 1.359(8) Å for molecule B are significantly shorter than the sp^3 single bond value of 1.533 Å.[48]

It is difficult to derive any general conclusion about the differences in molecular dimensions because of several factors: the conjugation of the lone electron pair on N(3) with C(4)=O, or on S(7) with C(5)=C(6), electron delocalisation of different sorts and hydrogen bonding. The remarkable shortening reported for C(4)=O(8) in saturated pyrimidines[47–50] was also observed in the present dimeric structure. The C(2)=S(7) distance observed is shorter than for similar bonds in the thione form of thiopyrimidine.[43,45,47] The valence angles at N1 and N3 are larger than 120° and these N atoms have extra-annular H atoms, in accordance with observations cited elsewhere.[51] The least-squares plane calculation for the morpholine ring on MMTU (Table S2, ESI) shows that N10 and O13 are displaced on opposite sides, *i.e.* O13 and N10 are in endocyclic and exocyclic positions respectively in molecule A, whereas in molecule B O13 and N10 are in exocyclic and endocyclic positions, respectively. In both molecules S7, O8 and C9 of the thiouracil moiety significantly deviate from the mean plane of N1–C2–N3–C4–C5–C6. The thiouracil and morpholine rings are not in the same plane. The total puckering amplitude for thiouracil and morpholine was found to be 0.0375 and 0.5849 Å for molecule A and 0.0420 and 0.5818 Å for molecule B. In this structure we observe a different type of hydrogen bonding pattern (Fig. 2, Table S3, ESI) which differs from the characteristic pattern exhibited by pyrimidine analogs.[52,53] The molecules A and B are connected by hydrogen bonds C11–H11′ ··· O8′ and C15′–H15 ··· O8 of 2.527 and 2.531 Å, respectively forming random HB arrays. Two inter-molecular contacts H6 ··· S7 and H9 ··· S7 of 2.744 and 2.964 Å are seen which

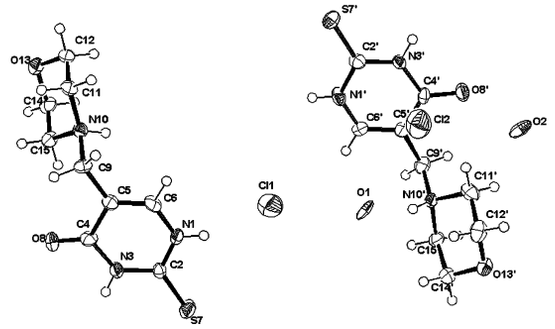

Fig. 1 ORTEP structure of MMTU·HCl.

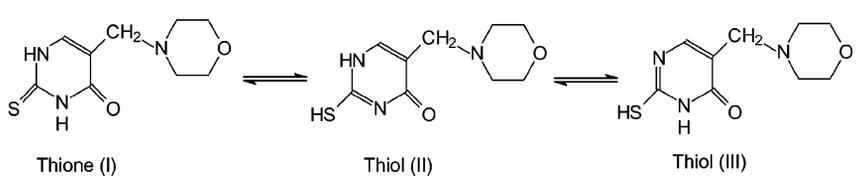

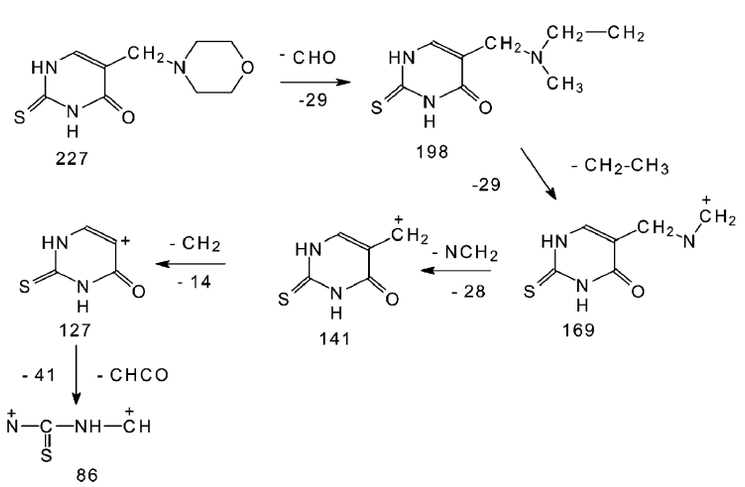

Table 1 Elemental analyses and molar conductance data for cobalt(II), nickel(II) and zinc(II) complexes of MMTU

Compound	Yield (%)	Elemental analyses (%) Carbon Obs. (calc.)	Hydrogen Obs. (calc.)	Nitrogen Obs. (calc.)	Sulfur Obs. (calc.)	Metal Obs. (calc.)	Anion Obs. (calc.)	Λ_M[a]/Ω^{-1} cm^2 mol^{-1}
$\cdots [N_3SO_2C_9H_{13}CoCl_2C_9H_{13}N_3SO_2] \cdots$	80	30.25 (30.27)	3.70 (3.67)	11.78 (11.77)	9.00 (8.98)	16.51 (16.50)	19.87 (19.85)	45
$[C_9H_{13}N_3SO_2CoBr_2]$	78	24.32 (24.23)	2.98 (2.94)	9.40 (9.42)	7.20 (7.19)	13.23 (13.21)	35.86 (35.83)	67
$[C_9H_{13}N_3SO_2CoI_2\,(H_2O)_2]$	71	18.79 (18.76)	2.95 (2.97)	7.28 (7.29)	5.56 (5.57)	10.25 (10.23)	44.00 (44.06)	67
$[C_9H_{13}N_3SO_2Co(NO_3)_2]$	82	26.35 (26.35)	3.18 (3.19)	17.08 (17.07)	7.81 (7.82)	14.40 (14.37)	— (30.25)	83
$[C_9H_{13}N_3SO_2{\cdot}CoSO_4(H_2O)_2]$	80	25.85 (25.84)	4.07 (4.10)	10.06 (10.04)	15.31 (15.33)	14.10 (14.09)	22.95 (22.96)	39
$[C_9H_{13}N_3SO_2{\cdot}NiCl_2(H_2O)_2]$	75	27.50 (27.51)	4.35 (4.36)	10.69 (10.69)	8.15 (8.16)	14.95 (14.94)	18.06 (18.05)	30
$[C_9H_{13}N_3SO_2{\cdot}Ni(H_2O)_2]$	67	18.79 (18.77)	2.95 (2.95)	7.29 (7.30)	5.58 (5.56)	10.21 (10.20)	44.12 (44.10)	155
$[C_9H_{13}N_3SO_2{\cdot}Ni(NO_3)_2(H_2O)_2]$	74	24.24 (24.23)	3.82 (3.84)	15.70 (15.70)	7.18 (7.18)	13.15 (13.14)	— (30.27)	81
$[C_9H_{13}N_3SO_2{\cdot}NiSO_4{\cdot}(H_2O)_2]$	77	25.92 (25.86)	4.10 (4.10)	10.00 (10.05)	15.35 (15.34)	14.05 (14.04)	22.98 (22.98)	64
$[(C_9H_{13}N_3SO_2)_2ZnCl_2{\cdot}H_2O]$	80	28.37 (28.33)	3.98 (3.96)	11.00 (11.01)	8.42 (8.40)	17.15 (17.14)	18.56 (18.58)	26
$[(C_9H_{13}N_3SO_2)_2{\cdot}Zn_2]Br_4$	78	23.90 (23.89)	2.91 (2.90)	9.31 (9.29)	7.10 (7.09)	14.45 (14.45)	35.33 (35.32)	162
$[(C_9H_{13}N_3SO_2)_2{\cdot}Zn_2(NO_3)_4]$	75	25.95 (25.94)	3.15 (3.14)	16.83 (16.81)	7.70 (7.70)	15.71 (15.69)	— (29.78)	30
$[C_9H_{13}N_3SO_2{\cdot}Zn_2(SO_4)_2]$	73	27.80 (27.81)	3.35 (3.37)	10.80 (10.81)	16.50 (16.50)	16.80 (16.82)	24.73 (24.71)	25

[a] In DMF solution.

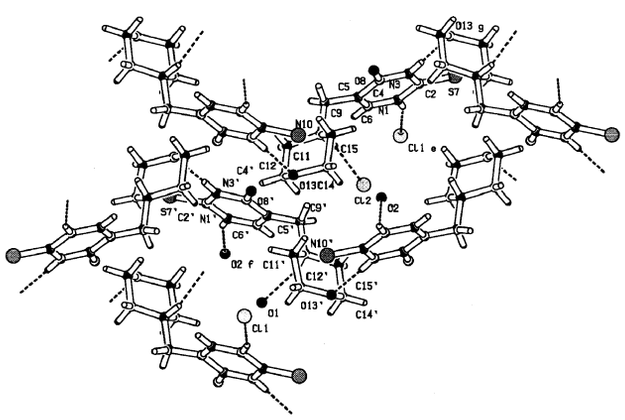

Fig. 2 Hydrogen bonding and stacking interactions of MMTU·HCl.

are lower than the H ⋯ S van der Waals distance of 3.05 Å.[54] The other two contacts of S7 with H11 and H14 are 3.102 and 3.005 Å, respectively. Pyrimidine oxygen atom O8 is only involved in the C–H ⋯ O type interaction.

Microelemental analyses and conductance measurements

The Λ_M values for 10^{-3} M DMF solutions of the nickel(II) iodide and zinc(II) bromide complexes suggest them to be 1 : 2 electrolytes and the remaining complexes are non-electrolytes. The analytical data for C, H, N, S, metal and anion content in the complexes are given in Table 1.

Infrared spectra

Comparison of the IR spectrum of MMTU with those of its complexes (Table 2, also see Figs. S4–S6, ESI) suggests the following. Perceptible shifts by about 50 to 100 and 52 to 90 cm^{-1} are observed in the $\nu_{C(4)O}$ and ν_{C-N-C} respectively in the case of cobalt(II) bromo, iodo, nitrato and sulfato and nickel(II) chloro, nitrato and sulfato complexes. In the IR spectra of the nickel(II) iodide and zinc(II) bromide complexes negative shifts in respect of $\nu_{C(2)S}$, $\delta_{N(3)H}$, $\nu_{C(4)O}$ and ν_{C-N-C} by about 104–108, 17–88, 30–100 and 27–91 cm^{-1} respectively, are observed. The stretching frequencies of the thiocarbonyl and carbonyl group exhibit negative shifts by about 85–107 and 40–80 cm^{-1} respectively, in the copper(II) sulfato and zinc(II) nitrato and sulfato complexes. In the IR spectrum of the zinc(II) chloro complex $\nu_{C(2)S}$, $\nu_{C(4)O}$ and ν_{C-N-C} bands are lowered by 104, 29 and 26 cm^{-1}, respectively. The cobalt(II) chloro complex exhibits negative shifts only in respect of C(4)O and N(1)H stretching and bending vibrations by about 85 and 62 cm^{-1}, respectively.

The diagnostic bands of the nitrato group in the case of cobalt(II) and zinc(II) complexes show a separation of ($\nu_5 - \nu_1$) = 100 cm^{-1} which indicates the monodentate mode of coordination. The IR spectrum of the nickel(II) nitrato complex exhibits bands at ~1500, ~1300 and ~1000 cm^{-1} which do not have any corresponding bands in the free ligand. These are assigned to ν_1, ν_5 and ν_2 modes of the coordinated nitrato group. The magnitude of $\nu_5 - \nu_1$ clearly indicates that the nitrato group is coordinated bidentately in these complexes.[55] All the sulfato complexes register new strong bands in the range of 1200–1290, 1125–1170 (ν_3); 860–980 (ν_1); 600–650 (ν_4) and 540–580 cm^{-1} (ν_2) which point to a bidentate mode of coordination for the sulfato group.[55] The cobalt(II) iodo and sulfato; nickel(II) chloro, sulfato and iodide and zinc(II) chloro complexes exhibit new non-ligand bands at 3400, 1620, 860, 820 and 760 cm^{-1} in the complexes indicating the presence of coordinated water.[55] In a few cases the ν_{OH} band has been masked by other broad bands in that region. However, the wagging and rocking modes of water occurring at 605 and 400 cm^{-1} respectively show the presence of coordinated water.

The above IR data indicate that MMTU exhibits six types of coordination pattern *viz*., bidentate through C(4)O and C–N–C; bidentate binuclear through C(2)S and C–N–C and C(2)S and C(4)O; tridentate binuclear through C(2)S, C(4)O and C–N–C; polymer of unidentate dimeric arrays involving N(1)H and C(4)O atoms; and tetradentate binuclear through C(2)S, N(3)H, C(4)O and C–N–C. Far IR band assignments further

Table 2 Important IR absorption bands (cm^{-1}) of cobalt(II), nickel(II) and zinc(II) complexes of MMTU

Compound	ν_{NH}	ν_{CH}	$\nu_{C=O}$	$\delta_{N(1)H}$	$\delta_{N(3)H}$	$\nu_{C=S}$	ν_{C-N-C}
$C_9H_{13}N_3SO_2$	3280m	3100m	1690s	1571_m	1473m	1225s	1102s
$\cdots [N_3SO_2C_9H_{13}CoCl_2C_9H_{13}N_3SO_2] \cdots$	3458m	3090m	1605s	1509m	1469m	1228s	1101s
$[C_9H_{13}N_3SO_2CoBr_2]$	3396b		1594s	1547m	1476m	1229s	1013m
$[C_9H_{13}N_3SO_2CoI_2\ (H_2O)_2]$	3420b		1591s	1542m	1468m	1194s	1012m
$[C_9H_{13}N_3SO_2Co(NO_3)_2]$	3423b		1595s	1545m	1465m	1220s	1015m
$[C_9H_{13}N_3SO_2{\cdot}CoSO_4(H_2O)_2]$	3420b		1595s	1570m	1475m	1129s	1020m
$[C_9H_{13}N_3SO_2{\cdot}NiCl_2(H_2O)_2]$	3460m	3050m	1620s	1575m	1470m	1220s	1025m
$[C_9H_{13}N_3SO_2{\cdot}Ni(H_2O)_2]I_2$	3422m	3222m	1645s	1586m	1456m	1117s	1053m
$[C_9H_{13}N_3SO_2{\cdot}Ni(NO_3)_2(H_2O)_2]$	3420b		1640s	1575m	1470m	1120s	1050m
$[C_9H_{13}N_3SO_2{\cdot}NiSO_4{\cdot}(H_2O)_2]$	3485b		1590s	1575m	1473m	1125s	1040m
$[(C_9H_{13}N_3SO_2)_2ZnCl_2{\cdot}H_2O]$	3800m	3029m	1661s	1560m	1470m	1121s	1076m
$[(C_9H_{13}N_3SO_2)_2{\cdot}Zn_2]Br_4$	3400m	3058m	1660s	1562m	1430m	1120s	1075m
$[(C_9H_{13}N_3SO_2)_2{\cdot}Zn_2(NO_3)_4]$	3400m	3060m	1610s	1565m	1470m	1140s	1100m
$[C_9H_{13}N_3SO_2{\cdot}Zn_2(SO_4)_2]$	3400m	3050m	1615s	1562m	1475m	1130s	1100m

s = Sharp, m = medium b = broad.

support the metal–heteroatom and metal–anion bonding suggested by the IR data.

Electronic spectra

Cobalt(II) complexes. The UV-Vis spectra of cobalt(II) chloro, bromo and nitrato complexes exhibit absorption bands (Table 3) in the visible and near IR region due to the transition from $^4A_2$ to $^4T_1(P)$ and $^4T_1(F)$, respectively. These transitions are characteristic of cobalt(II) in a tetrahedral environment.[56] The magnetic moments of the complexes lie in the range of 4.41–4.73 μ_B which again supports the tetrahedral environment around cobalt(II).[57] The percentage covalency for the cobalt(II) chloro, bromo and nitrato complexes are 35, 41 and 40, respectively. This observation can be explained on the basis of the polarisabilities of the anion. The LFSE (Table 3) for the complexes were found to be in the order: nitrato > chloro > bromo complexes. Electronic spectra of the cobalt(II) iodo and sulfato complexes exhibit bands corresponding to the transitions from $^4T_{1g}(F)$ to $^4T_{2g}$, $^4A_{2g}$ and $^4T_{1g}(P)$. The μ_{eff} values fall in the range 5.30–5.34 μ_B and the electronic spectral band positions indicate an octahedral coordination geometry for these complexes. The various ligand field parameters for the complexes are listed in Table 3. Among the halide complexes the ligand field splitting trend observed is $I^- > Cl^- > Br^-$. Among tetrahedral complexes the order of crystal field splitting is found to be $Br^- < Cl^- < NO_3^-$ which is in accordance with their positions in the spectrochemical series.

Nickel(II) complexes. The chloro, iodide, sulfato and nitrato complexes have a magnetic moment of 3.34 to 3.65 μ_B suggesting an octahedral environment. Three electronic absorption bands are seen (Table 3) in all the nickel(II) complexes. Their energy positions characterise the ground state as $^3A_{2g}$ thereby supporting the distorted octahedral geometry which is also reinforced by their ν_2/ν_1 values. The coordination environment of the iodide and chloro complexes are 2N, 3O and 1S and 1N, 3O and 2Cl, respectively. Apart from O and N, the other donor atoms are S and Cl. The position of S is lower compared to Cl in the spectrochemical series and hence the Dq value is lower for the iodide complex. The ν_2/ν_1 ratios for the various nickel(II) complexes are in very close agreement with the values expected for nickel(II) in an octahedral environment.

^{1}H NMR spectra

In the ^{1}H NMR of zinc(II) chloro (Fig. S7, ESI) and bromide complexes, the $-N-(CH_2)_2$ signal experiences a downfield shift due to the deshielding effect and a consequent electron drift from the nitrogen to the metal centre upon coordination, thereby supporting the coordination of the ligand through C–N–C of the amino moiety as suggested from IR data. IR spectra of zinc(II) nitrato and sulfato complexes suggest coordination through the C(4)O and C(2)S and accordingly no major shifts in the positions of NMR signals are observed in these cases. The zinc(II) chloro complex registers an additional signal at δ 4.08–4.18 confirming the presence of coordinated water in this complex.

Based on microelemental analyses, conductance measurements, IR, UV-Vis, magnetic moment measurements and ^{1}H NMR the following are the tentative structures proposed for the complexes:

Semi-empirical quantum mechanical calculations

The optimized geometry of MMTU is shown in Fig. 3. The

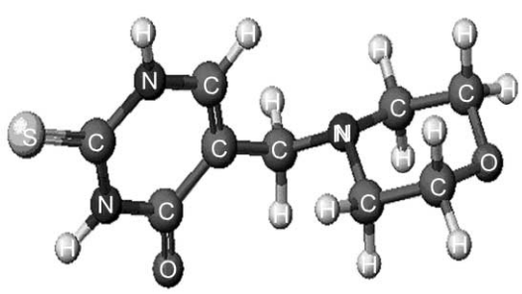

Fig. 3 Optimized geometry of MMTU for M.O. calculations.

results of the calculations (Table S4, ESI) show that there are 41 filled levels, the HOMO has an energy of 9.20756 eV. The negative value of this energy level is the ionization potential, in accordance with Koopman's theorem. Analysis of the corresponding eigenvector shows that it is mainly due to the lone pair on oxygen. The eigenvector forms an orthonormal set. The presence of a *z*-dipole indicates that the molecule is not flat or planar. The barriers of rotation were calculated by twisting the molecule about the bond or bonds in question and at each point, the geometry with respect to all other geometric variables was optimized. From the magnitude of energy involved in rotation, it was possible for us to correlate with the thermal decomposition patterns. The bonds, which require less energy, are cleaved first and *vice versa*. The gradient normalization energy for various bonds, bond angles and dihedral angles also correlate well with the thermal decomposition pattern (Fig. S8, ESI). Comparison of the magnitude of energy involved for a variation in bond length and angles gives an indication that the decomposition has to originate from the carbon atom of the amino moiety which has a weak bond. An analogous trend was also observed in the mass spectral fragmentation pattern.

The electron density order for the ligand was found to be C(4)O > C(2)S > C–O–C > N(3)H > N(1)H > C–N–C. Based

Table 3 Colour, electronic spectral bands, transition assignments, magnetic moments and ligand field parameters for cobalt(II) and nickel(II) complexes of MMTU

Parameter	$CoCl_2 \cdot L$	$CoBr_2 \cdot L$	$CoI_2 \cdot L \cdot 2H_2O$	$Co(NO_3)_2L$	$CoSO_4 \cdot L \cdot 2H_2O$	$NiCl_2 \cdot L \cdot 2H_2O$	$NiI_2L \cdot 2H_2O$	$Ni(NO_3)_2 \cdot L$	$NiSO_4 \cdot L \cdot 2H_2O$
Colour	Blue	Blue	Greyish pink	Green	Pink	Green	Pale green	Pale green	Pale green
μ_{eff}/μ_B	4.41	4.66	5.34	4.73	5.30	3.40	3.65	3.34	3.50
Environment	1N, 1O and 2 Cl	1N, 1O and 2 Br	1N, 3O and 2I	1N and 3O	1N and 5O	1N, 3O and 2 Cl	2N, 3O and 1 S	1N and 5O	1N and 5O
ν_1/cm^{-1} ($\varepsilon_{max.}/M^{-1}\ cm^{-1}$)	4086[c,d]	3982[c,d]	7175[g] (7)	5743[c,d]	7335[g] (8)	7902[j] (7)	7723[j] (6)	8200[j] (7)	8167[j] (7)
ν_2/cm^{-1} ($\varepsilon_{max.}/M^{-1}\ cm^{-1}$)	7000[e] (75)	6780[e] (72)	15468[h] (1)	9452[e] (55)	15740[h] (1)	13135[k] (6)	12730[k] (8)	13793[k] (8)	13.736[k] (9)
ν_3/cm^{-1} ($\varepsilon_{max.}/M^{-1}\ cm^{-1}$)	14700[f] (400)	13699[f] (405)	19800[i] (13)	16667[f] (385)	19200[i] (15)	23400[l] (16)	22026[l] (15)	25750[l] (16)	25641[l] (15)
ν_3/ν_2	2.100	2.021	1.280	1.763	1.220	1.78	1.73	1.87	1.87
ν_3/ν_1	3.598	3.440	2.760	2.902	2.618	2.96	2.85	3.14	3.14
ν_2/ν_1	1.713	1.703	2.156	1.646	2.146	1.66	1.65	1.68	1.68
ν_3/B	23.379	24.083	21.630	28.52	22.26	27.38	28.52	25.89	25.89
B/cm^{-1}	628.77	568.82	915.39	584.40	862.53	854.64	772.27	994.59	990.46
Dq/B	0.65	0.70	0.90	1	0.975	0.925	1	0.825	0.830
Dq/cm^{-1}	408.7	398.17	823.86	584.40	840.97	790.54	772.27	820.54	822.08
β[a]	0.65	0.59	0.94	0.60	0.89	0.82	0.74	0.95	0.95
$\beta/°$	35	41	6	40	11	18	26	5	5
LFSE[b]/kcal	14.01	13.65	28.25	20.04	28.83	27.10	26.48	28.13	28.19

L = 5-Morpholinomethyl-2-thiouracil.[a] $\beta = B$(complex)/B(free ion). Free ion value for Co^{II} = 971 cm^{-1}; Free ion value for Ni^{II} = 1041 cm^{-1}. [b] LFSE = 12 Dq; 1 kcal mol^{-1} = 350 cm^{-1}. [c] Calculated absorption band. [d] $^4T_2 \longleftarrow {}^4A_2$. [e] $^4T_1(F) \longleftarrow {}^4A_2$. [f] $^4T_1(P) \longleftarrow {}^4A_2$. [g] $^4T_{2g} \longleftarrow {}^4T_{1g}(F)$. [h] $^4T_{2g} \longleftarrow {}^4T_{1g}(F)$. [i] $^4T_{1g}(P) \longleftarrow {}^4T_{1g(F)}$. [j] $^3T_{2g} \longleftarrow {}^3A_{2g}(\nu_1)$. [k] $^3T_{1g}(F) \longleftarrow {}^3A_{2g}(\nu_2)$. [l] $^3T_{1g}(P) \longleftarrow {}^3A_{2g}(\nu_2)$.

on the above order for a bidentate mode of chelation, the donor atoms are C(4)O and C(2)S. For a tridentate mode of coordination one of the options for the donor atom is morpholine oxygen and the involvement of this atom in complex formation may not be feasible because the oxygen atom is exocyclic with respect to the thiouracil plane and a conformational change has to occur if oxygen has to be involved in coordination. The next obvious choice is N(3)H and for other higher denticities preferences will be N(1)H, C–N–C in that order. The above prediction regarding the donor atoms holds good for the complexes having a d^{10} configuration. The discrepancies in the predictions occur for d^7 and d^8 metal ions, they follow a random order. This behaviour might be due to inter-electron repulsion, however, the involvement of the pair C(4)O and C–N–C (morpholine nitrogen) is due to the additional stability achieved by the formation of a six membered chelate even though C–N–C is a poor electron donor among the predicted donor atoms.

Calculations of thermodynamic quantities using determined vibrational frequencies indicates some deviations when compared with the experimentally observed vibrational frequencies. Many of the errors in calculating vibrational frequencies were systematic, similar deviations occur for a given type of vibration in the molecule. However, for a few vibrations the deviations may be both because of their large number and the complexities which arise from the numerous combination and overtone bands possible in the system. Since a systematic variation exists between the calculated and observed vibrational frequencies, a rigorous quantum mechanical scaling method needs to be applied for correcting the vibrational frequencies and to calculate the various thermodynamic parameters.

Thermal decomposition and kinetic studies

The important features of the TG/DTA curves and the various stages of decomposition are given in Table 4. The examination of thermograms indicates a multistage decomposition involving loss of coordinated water molecules, oxidation of the organic moiety and formation of metal oxides. The derivative thermograms of all the complexes are characterized by an intense sharp peak for the last stage decomposition (see Fig. S9, ESI, for a representative example). The thermal parameters for the various decomposition stages are given in Table 5. In the majority of the metal complexes, the last stage decomposition corresponds to the formation of metal oxide. The activation energies for the last stage of decomposition in the complexes are higher than for all the other earlier stages of thermal decomposition. The difference in the activation energy values for the different stages may be due to the different types of decomposition mechanism operating in different temperature zones. The magnitude of the activation energy is primarily influenced by the mechanistic pathway of the decomposition. In general, a chemically controlled reaction mechanism is known to exhibit a higher activation energy and a pore diffusion controlled reaction mechanism, a lower value. Therefore, in the present study the initial stages of the thermal decomposition of the compounds may correspond to a mechanistic pathway involving the diffusion-controlled mechanism thereby resulting in a lower activation energy value for the decay.[58] Once the water/organic moiety is eliminated from the complex, many pores may be formed over the surface and at higher temperature, the reaction mechanism is chemically controlled resulting in higher activation energies for the formation of metal oxides. The negative values of $\Delta S^{\#}$ show that the complexes are more ordered in the activated state than the reactants and the reactions are slower as indicated by the TG curve at the corresponding temperature. The positive $\Delta S^{\#}$ of the complexes indicates that the activated state is less ordered in structure compared with the reactants and the reactions may be fast as indicated by rapid mass loss in the thermograms.

Unidentate dimeric arrays

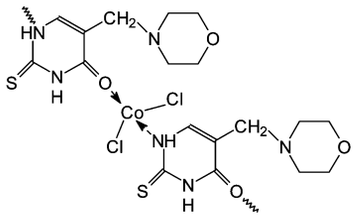

Bidentate

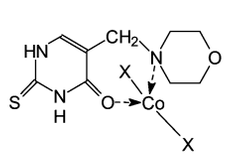

X = Br & NO_3

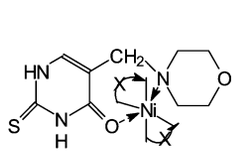

X = NO_3

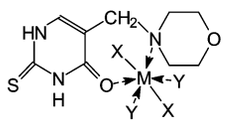

M = Co; X = I; Y = H_2O
M = Co & Ni; X = 1/2 SO_4; Y = H_2O
M = Ni; X = Cl; Y = H_2O

Bidentate binuclear

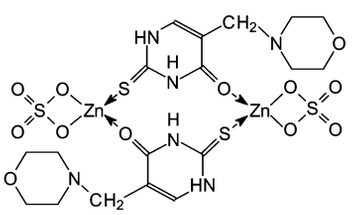

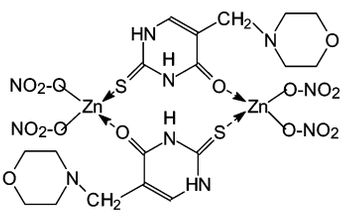

Tridentate binuclear

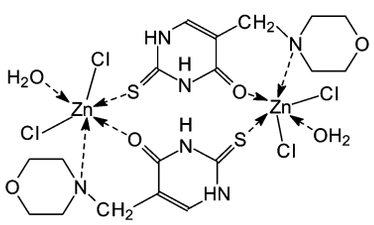

Tetradentate binuclear

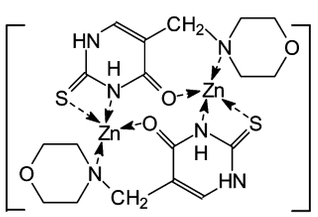

Br_4

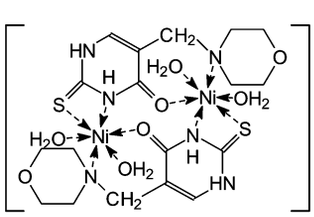

I_4

Biological studies

Antibacterial activity. Among the compounds tested, the cobalt(II) bromo complex was found to be the most active against *S. aureus* and *E. coli* (Table 6). The activity of the cobalt(II) complex may be due to its interaction with RNA. Also cobalt(II) is an essential micronutrient during transcription and transformation. The order of activity was found to be cobalt(II) bromo complex > cobalt(II) chloro complex > zinc(II) sulfato complex > zinc(II) chloro complex > nickel(II) iodide complex > standard > MMTU. It was found that the metal ion complexes were more biologically active than MMTU in all cases. It was also observed that there existed some relationship between the lability (as discerned from thermal studies) of M–O, M–N, M–S and M–X (X = anionic counter part of the metal ion) and the biological activities; *viz*. the activity increased with increasing lability of the metal complexes. Among the complexes the thermally labile ones were found to be more active. The steric constraints are less for a tetrahedral than for an octahedral complex and we observed that the tetrahedral complexes are more active than the octahedral ones.

Antifungal studies. MMTU was found to be less active compared to its metal ion complexes with $Co(NO_3)_2$·MMTU being found to be the most active. The zones of inhibition exhibited by these complexes are presented in Table 7. A possible mechanism of antifungal activity may be speculated in the light of chelation theory.[59] Chelation considerably reduces the polarity of the metal ion mainly because of partial sharing of its positive charge with donor groups and possible π-delocalisation over the chelate ring. This increases the lipophilic character of the neutral chelate which favours its permeation through the lipid layers of fungus membranes. Furthermore, the mechanism of action of the compounds may involve the formation of

Table 4 TG/DTG/DSC data, activation energy, entropy for cobalt(II), nickel(II) and zinc(II) complexes of MMTU

Compound	Stages	Decomposition temperature range/ K (°C) Initial	Final	Probable intermediate (calc. %) obs. %[a]	Nature of the DSC peak	DTG peak/K
$C_9H_{13}N_3SO_2$	Stable up to	473 (200)		Phase transformation	Endothermic	
	Stage I	473 (200)	523 (250)	Four membered cyclic compound (R)		508
	Stage II	673 (400)	713 (440)	Oxidative degradation (G)	Exothermic	688
	Stage III	713 (440)	853 (580)	Volatilisation (R)	Exothermic	788
$[C_9H_{13}N_3SO_2CoBr_2]$	Stable up to	353 (80)		Phase transformation	Endothermic	
	Stage I	353 (80)	393 (120)	Reductive elimination of Br; (82.07) 82.00; (S)	Exothermic	533
	Stage II	723 (500)	848 (575)	CoO (16.81) 17.00 (R)	Exothermic	763
$[C_9H_{13}N_3SO_2{\cdot}Ni(H_2O)_2]I_2$	Stable up to	353 (80)		NiI_2·MMTU; (93.33) 93.00; (G)	Endothermic	
	Stage I	468 (198)	573 (300)	Oxidative degradation (G)	Exothermic	493
	Stage II	583 (310)	693 (420)	(G)	Exothermic	628
	Stage III	723 (450)	773 (500)	NiO (13.84) 14.00 (G)	Exothermic	753
$[(C_9H_{13}N_3SO_2)_2ZnCl_2{\cdot}H_2O]$	Stable up to	413 (140)		$ZnCl_2$·MMTU; (95.28) 95.00	Endothermic	
	Stage I	498 (225)	773 (500)	Oxidative degradation (S)	Exothermic	588
	Stage II	813 (540)	873 (600)	ZnO (21.33) 21.00 (R)	Exothermic	843

[a] R = Rapid mass loss, G = gradual mass loss, S = slow mass loss.

Table 5 Activation energy, entropy, free energy and enthalpy for the thermal decomposition data of MMTU and its complexes by the Coats–Redfern and Madhusudanan–Krishnan–Ninan equations

		CR equation					MKN equation				
Compound	Stage	E_a/kJ mol^{-1}	$\Delta S^{\#}$/J K^{-1} mol^{-1}	$\Delta G^{\#}$/kJ mol^{-1}	$\Delta H^{\#}$/kJ mol^{-1}	r	E_a/kJ mol^{-1}	$\Delta S^{\#}$/J K^{-1} mol^{-1}	$\Delta G^{\#}$/kJ mol^{-1}	$\Delta H^{\#}$/kJ mol^{-1}	r
$C_9H_{13}N_3SO_2$	I	259.04	303.73	96.29	250.59	0.9992	259.10	303.30	96.58	250.65	0.9993
	II	159.14	11.31	139.92	147.70	0.9996	159.43	11.43	140.12	147.99	0.9996
	III	144.51	−45.10	166.95	131.41	0.9999	147.37	−44.69	169.48	134.26	0.9999
$[C_9H_{13}N_3SO_2CoBr_2]$	I	7.64	−211.79	84.34	1.11	0.9983	7.64	−214.63	85.45	1.10	0.9984
	II	161.65	−12.78	158.71	148.96	0.9989	161.49	−17.61	162.23	148.80	0.9989
$[C_9H_{13}N_3SO_2{\cdot}Ni(H_2O)_2]I_2$	I	19.72	−174.90	97.75	11.52	0.9988	19.70	−178.35	99.43	11.50	0.9988
	II	63.35	−127.40	132.91	52.91	0.9999	63.29	−131.62	135.50	52.84	0.9999
	III	586.58	556.27	155.19	574.06	0.9989	585.99	550.60	158.87	573.47	0.9989
$[(C_9H_{13}N_3SO_2)_2ZnCl_2{\cdot}H_2O]$	I	21.33	−200.34	129.36	11.55	0.9998	21.31	−203.85	131.40	11.53	0.9999
	II	348.77	187.13	177.00	334.75	0.9997	348.42	181.80	181.15	334.40	0.9998

Table 6 Antibacterial activity (% inhibition) of MMTU and its complexes against *Staphylococcus aureus* and *Escherichia coli*

	S. aureus				*E. coli*			
	Concentration of compound/μg mL^{-1}				Concentration of compound/μg mL^{-1}			
	25	50	75	100	25	50	75	100
Compound	% Inhibition				% Inhibition			
$C_9H_{13}N_3SO_2$	52	59	65	71	50	58	70	80
$[C_9H_{13}N_3SO_2CoBr_2]$	78	83	90	98	62	71	85	97
$\cdots [N_3SO_2C_9H_{13}CoCl_2C_9H_{13}N_3SO_2] \cdots$	70	81	88	95	60	69	80	94
$[C_9H_{13}N_3SO_2{\cdot}Ni(H_2O)_2]I_2$	56	63	72	81	52	62	73	85
$[(C_9H_{13}N_3SO_2)_2ZnCl_2{\cdot}H_2O]$	62	70	78	86	56	66	78	89
$[C_9H_{13}N_3SO_2{\cdot}Zn_2(SO_4)_2]$	65	73	81	88	60	70	80	90
Standard[a]	58	63	68	74	48	57	68	78

[a] Streptomycin for *S. aureus* and bezyl pencillin for *E. Coli*.

hydrogen bonds through the uncoordinated heteroatoms O, S and N with the active centres of the cell constituents resulting in interference with the normal cell processes. The presence of lipophilic and polar substituents such as C=O, C=S, and NH are expected to enhance the fungal toxicity and therefore these compounds have a greater chance of interaction with the nucleotide bases, biologically essential metal ions present in the biosystem, coordinatively unsaturated metals present in the metal ion complexes or with some of the enzymatic functional groups. The low activity of some of the complexes may be due to a mismatching of the geometry and charge distribution around the molecule with that around the pores of the fungal cell wall preventing penetration and hence toxic reaction within the pores. As a corollary, the complex cannot reach the desired site of action on the cell wall to interfere with normal cell activity.

Antitumour screening. The results obtained for MMTU and its complexes of cobalt(II), nickel(II) and zinc(II) on the growth of P-338 leukemic and Dalton's lymphoma cells are given in Table 8. In general, an increase in growth inhibition was observed as the concentration of test compound increased. Here also metal ion complexes show more activity than the ligand. The increase of activity on complexation is considerable

Table 7 Antifungal activity of MMTU and its complexes

Compound	Conc./μg mL^{-1}	Zone of inhibition/mm	Compound	Conc./μg mL^{-1}	Zone of inhibition/mm
$C_9H_{13}N_3SO_2$	0.2	12	$[C_9H_{13}N_3SO_2{\cdot}Ni(H_2O)_2]I_2$	0.2	14
	0.4	16		0.4	19
	0.6	24		0.6	26
$\cdots [N_3SO_2C_9H_{13}CoCl_2C_9H_{13}N_3SO_2] \cdots$	0.2	12	$[C_9H_{13}N_3SO_2{\cdot}NiCl_2(H_2O)_2]$	0.2	14
	0.4	22		0.4	18
	0.6	28		0.6	26
$[C_9H_{13}N_3SO_2CoI_2(H_2O)_2]$	0.2	12	$[(C_9H_{13}N_3SO_2)_2ZnCl_2{\cdot}H_2O]$	0.2	13
	0.4	22		0.4	24
	0.6	26		0.6	30
$[C_9H_{13}N_3SO_2Co(NO_3)_2]$	0.2	17	$[C_9H_{13}N_3SO_2{\cdot}Zn_2(SO_4)_2]$	0.2	15
	0.4	29		0.4	27
	0.6	34		0.6	32

in the case of the zinc(II) complex whereas the other complexes show moderate activity but higher than for free MMTU.

The percentage increase of life span (%ILS) of mice bearing leukemic and lymphoma cells due to MMTU and its cobalt(II), nickel(II) and zinc(II) complexes is given in Table 8. The zinc(II) sulfato complex was found to be most active among the complexes. Hydrogen bonding may also be an important factor in the antitumour mechanism. Adenine, guanine and cytosine have amine groups adjacent to an unprotonated ring nitrogen atom and are well positioned to form hydrogen bonds with these compounds (drugs) and thereby inhibit normal cell metabolism. Moreover, the presence of an endogenous receptor site, *viz*. oxygen, is free in the terminal position of the compound and hence the activity is increased.

The order of activity is MMTU < $NiI_2{\cdot}$MMTU < $CoBr_2{\cdot}$MMTU < $ZnCl_2{\cdot}$MMTU$\cdot H_2O$ < $ZnSO_4{\cdot}$MMTU. The free MMTU does not effectively reach the cancer cells and consequently less active. However, among the complexes screened the enhanced activity of the zinc(II) chelate can be explained as follows. A considerable amount of zinc is needed for rapidly dividing tumour cells, this zinc uptake tendency by cancerous cells leads to an easy uptake of the compound by cancerous cells. After reaching the receptor site the labile Zn–N or Zn–O or Zn–S bonds in the complexes undergo dissociation and produce free active antimetabolite, which is active in its own right. Comparing activities of these compounds against the two cell systems, leukemic cells were found to be relatively more resistant than lymphoma cells as the percentage of growth inhibition is greater in the latter case. The coordinatively unsaturated tetrahedral complex is more active than the octahedral complex.[60,61] From the present study it is seen that there is a relationship between the lability of M–O and M–N linkages and biological activity. The activity is directly proportional to the lability of the metal ion–MMTU bond.

Experimental

Materials

All the reagents used for synthesizing MMTU and its complexes were of A.R. grade and the solvents used were commercial products of the highest available purity and were further purified by distillation.

Synthesis of MMTU and its metal ion complexes

An equimolar mixture of 2-thiouracil (12.8 g), paraformaldehyde (3.0 g) and morpholine (8.8 g) was suspended in 400 mL of ethanol and refluxed for about 20 h. The clear homogeneous solution obtained was concentrated to 200 mL by distillation. On cooling the concentrate yielded a colourless crystalline solid (crude product 21.2 g; 93.4% yield) which was filtered, washed first with ethanol and then with ether. The compound was crystallised from methanol.

All the complexes were isolated from non-aqueous media. The cobalt(II), and nickel(II) bromo and nitrato; cobalt(II) iodo and nickel(II) iodide complexes were synthesized by mixing a 2-propanolic solution of the ligand with an ethanolic solution of the metal salt in a 2 : 1 molar ratio at 70 °C. The complexes precipitated in the form of insoluble products on cooling. The precipitated complexes were washed first with hot (70 °C) 2-propanol and then ethanol and dried in a vacuum oven. Ethanol was used as the medium for synthesizing the d^7 and d^8 metal sulfato and chloro complexes. Ethanol and methanol were used as the solvents for the ligand and the d^{10} metal salts, respectively.

Elemental analyses (C, H, N and S) were performed using a FISONS-CHNS/O elemental analyser. The purity of the ligand was checked using a Shimadzu LC10AT HPLC instrument fitted with an ODS column in the isocratic elution mode using 1 : 1 methanol–acetonitile as eluent. The mass spectral study of MMTU was carried out using a Finningan MAT-8230 mass spectrometer. After decomposing the complexes with HNO_3, the metal ion contents were determined using a GBC 902 AAS with an acetylene/air flame. The anion contents were estimated by standard literature procedures. The infrared spectral measurements for MMTU and its metal ion complexes were recorded as KBr discs and on a polyethylene support for the conventional and the far IR regions respectively using Ratio Recording Perkin-Elmer 1430 and Brucker IFS66V FT-IR spectrometers. The UV-Vis spectra were recorded using a JASCO 7800 UV-Vis double beam spectrophotometer in DMF solvent and a Hitachi U-3400 UV-Vis–NIR spectrophotometer which also covers the near IR region. Room temperature magnetic measurements of the complexes were carried out using a Gouy magnetic balance. The Gouy tube was calibrated using mercury(II) tetrathiocyanatocobaltate(II), as recommended by Figgis and Nyholm. Diamagnetic corrections for various atoms and structural units were computed from Pascal's constants. The effective magnetic moments were calculated from the corrected molar magnetic susceptibilities of the complexes using Curie's relation. The ^{1}H NMR of MMTU and its d^{10} metal ion complexes were recorded on JEOL GSX400NB 400 MHz FTNMR spectrometer employing TMS as internal reference and DMSO-d_6 as solvent at ambient temperature. The thermal studies (TG/DSC) were carried out on a Du Pont 910 DSC system with the 1090 programmer/data analyser in an atmosphere of air at a linear heating rate of 10 °C min^{-1} from ambient to 1000 °C using alumina as the standard reference material.

XRD data collection and determination of molecular topology

MMTU was dissolved in 1 : 1 acetic acid–water and a few drops of hydrochloric acid was added. Colourless crystalline solid separated out after a week, which was washed first with ethanol and then with acetone and dried under vacuum. Crystals showing good extinction under a polarizing microscope were used

Table 8 Cytotoxic action, growth inhibition studies (percentage dead cells) and %ILS (percentage increase of lifespan) of MMTU and its complexes on P-388 leukemic and Dalton's lymphoma cells

	Dalton's lymphoma cells								P-388 leukemic cells							
	Cytotoxic action concentration/ μg mL^{-1}				Growth inhibition concentration/ μg mL^{-1}					Cytotoxic action concentration/ μg mL^{-1}				Growth inhibition concentration/μg mL^{-1}				
Compound	25	50	75	100	10	20	30	40	50	% ILS	25	50	75	100	10	20	30	40	50	% ILS
$C_9H_{13}N_3SO_2$	48	58	67	76	40	48	56	62	70	48	32	37	43	50	25	30	35	37	40	20
$[C_9H_{13}N_3SO_2CoBr_2]$	59	63	75	87	47	53	62	74	83	80	40	46	53	60	35	40	44	48	52	30
$[C_9H_{13}N_3SO_2{\cdot}Ni(H_2O)_2]I_2$	52	60	71	80	43	50	60	70	80	75	36	42	49	56	30	35	41	45	50	25
$[(C_9H_{13}N_3SO_2)_2ZnCl_2{\cdot}H_2O]$	63	72	82	90	54	60	68	77	86	86	42	50	59	69	37	41	46	50	57	37
$[C_9H_{13}N_3SO_2{\cdot}Zn_2(SO_4)_2]$	68	76	85	96	60	68	76	84	92	91	49	59	70	80	42	48	53	59	65	42

Table 9 Crystal data and structure refinement for MMTU·HCl

Identification code	MMTU
Empirical formula	$C_9H_{16}ClN_3O_3S$
Formula weight	281.80
Temperature/K	293(2)
Wavelength/Å	0.71070
Crystal system, space group	Monoclinic, $P2_1$
a/Å	9.1416(14)
b/Å	13.412(2)
c/Å	10.6570(12)
β/°	106.647(14)
Volume/Å^3	1251.9(5)
Z	4
Absorption coefficient/mm^{-1}	0.473
F(000)	591.9
Crystal size/mm	0.32 × 0.27 × 0.24
Reflections collected/unique	2305/2083 [*R*(int) = 0.0161]
Refinement method	Full-matrix least-squares on F^2
Final *R* indices [$I > 2\sigma(I)$]	*R*1 = 0.052, *wR*2 = 0.162
R indices (all data)	*R*1 = 0.057, *wR*2 = 0.169

for data collection with an ENRAF-NONIUS CAD 4 diffractometer employing Mo-Kα radiation. Absorption corrections were applied to the data using *Ψ* scan method. The cell parameters and analysis over the data set indicate that the compound belongs to the monoclinic system and the systematic absences of *k* odd reflections in the 0 *k* 0 series revealed a 2_1 screw perpendicular to the *b*-axis. Accordingly the space group $P2_1$ was assigned to the compound. All the non-hydrogen atoms were located from the first electron density map itself, which led to an *R* value of 20.2%. After eleven cycles of full matrix least-squares adjustment of the coordinates and isotropic temperature factors the *R* value converged to 11.5%. The difference map indicated the location of all the hydrogens, except water hydrogens. Anisotropic refinement was then carried out. All the coordinates and isotropic temperature factors were included in the final refinement. The refinement was completed at $R = 0.0574$ for all 2305 reflections with $F_o > 4\sigma(F_o)$. The weighting scheme employed for the final cycle of refinement was:

$$W = 1/[\sigma^2(F_o^2) + (0.1072P)^2 + 1.52P],$$

where $P = [\max\{F_o^2, 0\} + 2F_c^2]/3$.

The intensity data sets were subjected to Lorentz polarization and absorption corrections using the MolEN program.[62] The structure was solved by direct methods[63] using the SHELXS 97 program[64] and refined by full-matrix least-squares methods on F^2 using the SHELXL 97 program. The geometric calculations were performed using the program PARST.[65,66] The hydrogen bonding and stacking interactions were calculated using PLATON.[67] The molecular structures were drawn using ORTEP.[68] All calculations were carried out using a HP-Vectra system. Data collection and refinement details are summarised in Table 9.

CCDC reference number 172362.

See http://www.rsc.org/suppdata/dt/b2/b202127g/ for crystallographic data in CIF or other electronic format.

Semi-empirical quantum mechanical calculations

Calculations were performed for MMTU and its zinc(II) complexes in order to gain theoretical support for its observed behaviour on complex formation and to evaluate parameters such as electronic energy, core–core repulsion, gradient norm, dipole, number of filled levels, ionization potential, results of SCF calculations, charge on each atom, eigen values, atomic charges, atom electron density and atomic electron population. The input data from the crystal structure were optimized by minimizing their total energy with respect to the corresponding geometric variables. The optimized geometry is in good agreement with the experimental data. The error in bond lengths is less than 0.2 Å and in bond angles less than 2°. Such errors are

not of great chemical significance[69] and attempts to reproduce the geometry much more accurately than this are not of any real value. Calculations were carried out using the parametric method-3 (PM-3) Hamiltonian and the program used for performing M.O. calculation was MOPAC version 6.00.[70] The geometry was optimized using the Broyden Fletcher–Goldfarb–Shanno (BFGS) method followed by Bartel's/Melver–Komornicki method and a self-consistent field is achieved. The eigen values, the diagonal elements of the Coulson density matrix representing the valence electron populations from each M.O, bonding contribution of each M.O., the charge and electron density on the atoms have also been calculated (see Tables S5–S9, ESI).

Calculations of thermodynamic quantities were carried out using vibrational frequencies determined by quantum mechanical methods using the keyword FORCE. Before proceeding to thermal calculation a check was made by calculating the gradient norm, if significant GNORM was reduced by BFGS. The keyword PRECISE was used to eliminate quatric contamination. M.O. calculations were also carried out for the zinc(II) complexes to explore the various bonding and physical parameters. The optimization terminated after 36 h in a PC with a P-IV processor. On analyzing the output geometry, it was observed that the optimization was not complete and required further refinement by imposing symmetry considerations which will be looked at as part of a further investigation.

Thermal decomposition and kinetic studies

Kinetic studies of the thermal decomposition of a few selected representative complexes have been carried out. The order parameters are determined using the iteration method and the kinetic parameters are evaluated using the Coats–Redfern (CR)[71] and Madhusudanan–Krishnan–Ninan (M–K–N)[72] equations. The correlation coefficient 'r' approaches unity for plots of the left hand side of the CR and MKN equations *vs.* $1/T$. The values of E_a, $\Delta S^{\#}$, $\Delta G^{\#}$ and $\Delta H^{\#}$ obtained by both methods are in very close agreement.

Antibacterial screening

The activity of the compounds synthesized were evaluated using a serial tube dilution technique.[73] These tests were performed in triplicate and activities of the compounds were cross-checked with the disc diffusion technique.[74] The compounds were screened for their antibacterial activity using *Staphylococcus aureus* and *Escherichia coli*. The former is a gram-positive organism, while the latter is gram-negative. The inhibition of growth of the gram-positive organism produced by various concentrations of test compounds was compared under identical conditions with the inhibition of growth of the same organism by benzyl penicillin. Similarly, the inhibition of gram-negative organism growth produced by the test compounds was compared with those for different concentrations of streptomycin. A solution of each test compound was prepared in DMF and a series of dilutions were prepared. The concentrations tested were 25, 50, 75 and 100 μg mL^{-1} of the compound under investigation, a standard antibiotic (streptomycin/benzyl pencillin), the respective metal salt dissolved in DMF and the blank (DMF). A control tube containing no test compound was also included. All these operations were carefully carried out under aseptic conditions. The assay tubes were incubated at 37 ± 1 °C. The resultant turbidities were measured in a Nephelo-turbidity meter. The relationship used for calculating the activity is:

$$\% \text{ Inhibition} = [(T_c - T_t)/T_t] \times 100$$

where T_c = turbidity of the control and T_t = turbidity of the specific treatment or the test compound.

Antifungal studies

Antifungal activities of these compounds were evaluated using the nutrient agar diffusion method and phenol as a reference standard. Wells were made (12 mm diameter) with a sterile cork borer. To these wells 0.2, 0.4, 0.6 mL (stock 1 mg mL^{-1}) of the test compound was added and the plates were allowed to cool for an hour to facilitate the diffusion. The plates were then incubated at 37 ± 1 °C for 48 h. At the end of the incubation period, the diameter of the zone of inhibition around the wells was measured.

Antitumour screening

***In vitro* cytotoxic studies.** The *in vitro* cytotoxicity assay was carried out using P-388 lymphocytic leukemic and Dalton's lymphoma cells and the Trypan blue dye exclusion method to measure viability. A stock solution (1 mg mL^{-1}) of compounds (MMTU and metal ion complexes in DMSO) was prepared. Different concentrations of complexes *i.e.*, 25, 50, 75 and 100 μg mL^{-1} were added in triplicate to test tubes and diluted to 0.9 mL. The same quantity of cell suspension (0.1 mL) was added and incubated in a CO_2 incubator at 37 °C for 3 h. A series of control tubes were also maintained without adding the test compound. After incubation, 0.3 mL of 0.4% Trypan blue solution was added to each tube and mixed gently. Since the Trypan blue will be absorbed only by dead cells, the number of dead cells and the percentage were estimated using a Hemocytometer.

Growth inhibition studies. Leukemic and lymphoma cells were used to determine the percentage growth inhibition by test compounds. Cells were collected after 7 days of transplantation from the tumour bearing mice and suspended in a culture medium to a cell density of 2×10^4 cells mL^{-1}. Varying concentrations of each complex and MMTU were added followed by incubation in a CO_2 incubator at 37 °C for 1 h. Cells were counted using a Hemocytometer by the Trypan blue exclusion method. The experiments were carried out in duplicate and the entire operation was carried out under aseptic conditions. The percentage growth inhibition is calculated by taking the total number of cells in the control tube (without test compound) as 100%.

***In vivo* antitumour evaluation of compounds.** Antitumour evaluation experiments were performed *in vivo* using groups of CDF mice and Swiss albino mice of either sex aged 6–8 weeks and 18–22 g body mass implanted with leukemic/lymphoma cells. A group of eight animals was treated as control and groups containing six animals were treated with test compounds. The animals were fed with normal mouse chow (Lipton India Ltd.) and water *ad libitum* and were housed in ventilated cages with husk as bedding material in air controlled rooms (25 °C). Two million cells were injected into the peritoneal cavity of Swiss albino mice and the Ascites tumour was allowed to grow. The test compounds were administered on the first, third and fifth day. The results are expressed as percentage increase in life span (%ILS) calculated as

$$[(T - C)/C] \times 100$$

where T = median survival time of treated animals and C = median survival time of control animals.

References

1 P. Kamalakannan and D. Venkappayya, *Proceedings of the 32nd Annual Convention of Chemists ING-YS-11*, Rajasthan, 1995.

2 P. Kamalakannan and D. Venkappayya, *Proceedings of the International Symposium on Recent Trends in Genetic Engineering*, TIFR–NCBS MIS-71, Bangalore, 1996.

3 P. Kamalakannan and D. Venkappayya, *Proceedings of the 34th Annual Convention of Chemists*, ING-OP-14: A6, Delhi, 1997.
4 P. Kamalakannan and D. Venkappayya, *Proceedings of the 35th Annual Convention of Chemists*, ING-OP-17: A6, Dharwad, 1998.
5 P. Kamalakannan and D. Venkappayya, *Proceedings of the 37th Annual Convention of Chemists*, ING-OP-03, Hardwar, 2000.
6 P. Kamalakannan and D. Venkappayya, *J. Inorg. Biochem.*, 2002, **90(1)**, 22–37.
7 K. Fuwa, W. E. C. Wacher and R. Duriyan, *Proceedings of National Academy of Sciences*, 1960, 1298–1307.
8 G. L. Eichhorn, *Met. Ions Biol. Syst.*, 1980, **10**, 1; G. L. Eichhorn, *Nature*, 1962, **194**, 474–475.
9 L. A. Leob and R. A. Zakour, *Nucleic Acid–Met. Ion Interact.*, 1980, **1**, 117.
10 C. P. Flessel, A. Furst and S. B. Radding, *Met. Ions Biol. Syst.*, 1980, **10**, 23.
11 M. S. Motawia, A. Megied, E. B. Pederson, C. M. Nielsen and P. Ebbesen, *Acta Chem. Scand.*, 1992, **46**, 77–81.
12 Y. Iwanami and G. M. Brown, *Arch. Biochem. Biophys.*, 1968, **124**, 472.
13 M. T. Abbot, R. J. Kander and R. M. Fink, *J. Biol. Chem.*, 1964, **239**, 156.
14 S. Fabrissin, M. DeNardo, C. Nisi, L. Morasca, E. Dolfini and G. Franchi, *J. Med. Chem.*, 1976, **19(5)**, 639–642.
15 T. Margot, F. Fakan and Z. Muchnova, *Neoplasma*, 1969, **16**, 249.
16 J. Slotova and Z. Karpfel, *Biol. Plant*, 1969, **11**, 49.
17 R. H. Lindsay, C. J. Romine and M. Y. Wong, *Arch Biochem. Biophys.*, 1968, **126**, 812.
18 R. Hamers and C. H. Casterman, *J. Med. Biol.*, 1972, **3**, 166–170.
19 J. Abbort, D. M. L. Goodgame and I. Jeeves, *J. Chem. Soc., Dalton Trans.*, 1978, 800–884.
20 I. Votruba, A. Holly and K. Jost, *FEBS Lett.*, 1972, **22**, 287–288.
21 E. R. Garrett and D. J. Weber, *J. Pharm. Sci.*, 1970, **59**, 1883.
22 M. S. Wysor and R. E. Zollinhofer, *Chemotherapy (Basel)*, 1972, **17**, 188.
23 C. A. Zittle, *J. Biol. Chem.*, 1946, **163**, 111.
24 K. Takamiya, *Nature*, 1960, **185**, 190–191.
25 J. Schubert, *Sci. Amer.*, 1966, **214**, 40–50.
26 B. Rosenberg and L. van Camp, *Nature*, 1969, **222**, 385–386.
27 B. Rosenberg and L. van Camp, *Cancer Res.*, 1970, **30**, 1799–1802.
28 K. H. Lee, E. S. Huang, C. Piantadosi, J. S. Pagano and T. A. Geissman, *Cancer Res.*, 1971, **31**, 1649–1654.
29 K. H. Lee, H. Furukawa and E. S. Huang, *J. Med. Chem.*, 1972, **15**, 609–611.
30 K. H. Lee, T. Ibuka and R. Y. Wu, *Chem. Pharm. Bull.*, 1974, **22**, 2206.
31 K. H. Lee, R. Meck, C. Piantadosi and E. S. Huang, *J. Med. Chem.*, 1973, **16**, 229–301.
32 S. M. Kupchan, D. C. Fessler, M. A. Eakin and T. J. Giacobbe, *Science*, 1970, **168**, 376.
33 K. H. Lee, Y. S. Wu and I. H. Hall, *J. Med. Chem.*, 1977, **20(7)**, 911.
34 M. Watnabe, N. Komeshina and S. Nakajima, *Cancer Res.*, 1988, **48**, 6653–6657.
35 S. A. Scudder, J. M. Brown and B. I. Sikic, *J. Natl. Cancer Inst.*, 1988, **80**, 1294–1298.
36 E. S. Raper, *Coord. Chem. Rev.*, 1985, **61**, 115–184.
37 D. Kovala-Demertzi, P. Kyrkon and I. Zakharoba, *Polyhedron*, 1991, **10**, 1507–1512.
38 Y. Wei-Da and H. Yin-Ping, *Polyhedron*, 1990, **22**, 2747–2750.
39 J. Abbot, D. M. L. Goodgame and I. Jeeves, *J. Chem. Soc., Dalton Trans.*, 1978, 880–884.
40 H. G. Mautner and G. Bergson, *Acta Chem. Scand.*, 1963, **17**, 1694–1704.
41 D. S. Wise and L. B. Townsend, *Tetrahedron Lett.*, 1977, **9**, 755–758.
42 J. P. Kokko, L. Mandell and J. H. Goldstein, *J. Am. Chem. Soc.*, 1961, **84**, 1042–1047.
43 B. Kojic-Prodic, Z. Ruzic-Toros and E. Coffou, *Acta Crystallogr., Sect. B*, 1976, **32**, 1099–1102.
44 D. C. Rohrer and M. Sundaralingam, *Acta Crystallogr., Sect. B*, 1970, **26**, 546–553.
45 E. Shefter and G. Mautner, *J. Am. Chem. Soc.*, 1967, **89**, 1249–1253.
46 R. F. Stewart and L. H. Jensen, *Acta. Crystallogr.*, 1967, **23**, 1102–1105.
47 S. Swaminathan and K. K. Chacko, *Acta Crystallogr., Sect. B*, 1978, **34**, 3108–3110.
48 L. S. Bartell, *J. Am. Chem. Soc.*, 1959, **81**, 3497–3498.
49 A. Banerjee, J. K. Dattagupta, W. Saenger and A. Rabczenko, *Acta. Crystallogr., Sect. B*, 1977, **33**, 90–94.
50 G. H. Y. Lin, M. Sundaralingam and S. K. Arora, *J. Am. Chem. Soc.*, 1971, **93**, 1235–1241.
51 C. Singh, *Acta. Crystallogr.*, 1965, **19**, 861–864.
52 D. Voet and A. Rich, *Prog. Nucleic Acid Res. Mol. Biol.*, 1970, **10**, 183–265.
53 C. E. Bugg, J. M. Thomas, M. Sundaralingam and S. T. Rao, *Biopolymers*, 1971, **10**, 175–219.
54 L. Pauling, *The nature of the chemical bond*, Cornell University Press, Ithaca, 1960.
55 K. Nakamoto, *Infrared and raman spectra of inorganic and coordination compounds*, 3rd edn., Wiley Interscience, New York, 1978.
56 A. B. P. Lever, *Inorganic electronic spectroscopy* . 2nd edn., Elsevier Science Publishers, Amsterdam, 1984.
57 B. N. Figgis and J. Lewis, *Modern coordination chemistry*, ed., J. Lewis and R. G. Wilkins, Interscience Publishers Inc., New York, 1960.
58 S. E. Smith, R. C. Neavel, E. J. Hippo and R. N. Miller, *Fuel*, 1981, **60**, 458–462.
59 R. S. Srivastava, *Inorg. Chim. Acta*, 1981, **56**, L65–L67.
60 A. Furst, *Chemistry of chelation in cancers*, C. Charles, Thomas Publishers, Illinois, 1963.
61 B. C. Bailer, *Metal complexes in cancer chemotherapy*, VCH, Weinheim, 1993.
62 Delft Instruments, MolEn structure determination system, Delft Instruments, X-ray diffraction, Roentgenweg, B. V., 1, 2624, BD Delft, The Netherlands, 1990.
63 G. H. Stout and L. H. Jenson, *X-ray Structure Determination, A Practical Guide*, John Wiley & Sons, New York, 1989.
64 G. M. Sheldrick, SHELXS 97, Programme for automatic structure solution and for refinement of crystal structure of crystal structure, University of Göttingen, Germany, 1997.
65 M. P. Nardelli, *Comput. Chem. (Oxford)*, 1983, **7**, 95.
66 M. P. Nardelli, *J. Appl. Crystallogr.*, 1995, **28**, 659.
67 A. L. Spek, PLATON, Bijvoet Centre for Biomolecular Research, University of Utrecht, Padualaan, The Netherlands, USA, 1999.
68 C. K. Johnson, ORTEPII. Report ORNL-5138, Oak Ridge National Laboratory, Tennessee, USA, 1976.
69 R. C. Bingham, M. J. S. Dewar and D. H. Lo, *J. Am. Chem. Soc.*, 1975, **97**, 1294–1301.
70 J. J. P. Stewart, *J. Comput.-Aided. Mol. Des.*, 1990, **4**, 1–45.
71 A. W. Coats and J. P. Redfern, *Nature*, 1964, **201**, 68–69.
72 P. M. Madhusudanan, K. Krishnan and K. N. Ninan, *Thermochim. Acta*, 1986, **97**, 189–201.
73 M. J. Pelczar, R. D. Reid and E. C. S. Chan, *Microbiology*, 4th edn., Tata Mc Graw-Hill, New Delhi, 1979.
74 R. S. Verma and W. L. Nobles, *J. Pharm. Sci.*, 1975, **64**, 881–887.